AIP | Chaos
An Interdisciplinary Journal of Nonlinear Science

Characterizing chaotic dynamics from simulations of large strain behavior of a granular material under biaxial compression

Michael Small, David M. Walker, Antoinette Tordesillas, and Chi K. Tse

Citation: Chaos **23**, 013113 (2013); doi: 10.1063/1.4790833
View online: http://dx.doi.org/10.1063/1.4790833
View Table of Contents: http://chaos.aip.org/resource/1/CHAOEH/v23/i1
Published by the AIP Publishing LLC.

Characterizing chaotic dynamics from simulations of large strain behavior of a granular material under biaxial compression

Michael Small,[1,a)] David M. Walker,[2] Antoinette Tordesillas,[2] and Chi K. Tse[3]
[1]*School of Mathematics and Statistics, The University of Western Australia, Crawley, WA 6009, Australia*
[2]*Department of Mathematics and Statistics, University of Melbourne, Parkville, VIC 3010, Australia*
[3]*Department of Electronic and Information Engineering, Hong Kong Polytechnic University, Hung Hom, Kowloon, Hong Kong*

(Received 27 August 2012; accepted 15 January 2013; published online 8 February 2013)

For a given observed time series, it is still a rather difficult problem to provide a useful and compelling description of the underlying dynamics. The approach we take here, and the general philosophy adopted elsewhere, is to reconstruct the (assumed) attractor from the observed time series. From this attractor, we then use a black-box modelling algorithm to estimate the underlying evolution operator. We assume that what cannot be modeled by this algorithm is best treated as a combination of dynamic and observational noise. As a final step, we apply an ensemble of techniques to quantify the dynamics described in each model and show that certain types of dynamics provide a better match to the original data. Using this approach, we not only build a model but also verify the performance of that model. The methodology is applied to simulations of a granular assembly under compression. In particular, we choose a single time series recording of bulk measurements of the stress ratio in a biaxial compression test of a densely packed granular assembly—observed during the large strain or so-called critical state regime in the presence of a fully developed shear band. We show that the observed behavior may best be modeled by structures capable of exhibiting (hyper-) chaotic dynamics. © *2013 American Institute of Physics*. [http://dx.doi.org/10.1063/1.4790833]

Inferring dynamical structure of a deterministic nonlinear system from noisy time series data is a long standing problem. Here, we demonstrate the application of a range of methods to a problem of particular interest in the study of granular materials. An initially dense assembly of grains under biaxial compression with constant confining pressure reaches a near steady-state behavior (modulo fluctuations) in the large strain regime. The dynamics of this system at this limit are the focus of this paper—and of significant interest within the soil mechanics literature. Understanding the dynamical response of the granular structure in this regime is crucial for prediction and control in many industrial and geophysical systems. Our analysis indicates that the dynamics of this system in the presence of a fully developed shear band are consistent with a form of transient chaos—characterized by a bistable system which switches between two chaotic regimes, one with large slow oscillations and one with smaller and faster dynamics.

I. INTRODUCTION

When an initially dense two-dimensional sample of granular material is biaxially compressed under a constant confining pressure, the load-carrying capacity of the sample, as measured by the macroscopic stress ratio $\frac{\sigma_{11}-\sigma_{22}}{\sigma_{11}+\sigma_{22}}$, and its macroscopic volume ε_{vol}, reaches a near steady-state condition in the large strain regime. It is the dynamics observed in this post-failure regime, sometimes referred to in the soil mechanics literature as the "critical state," that is of key interest in this study.[1] This limit state is posited, in critical state soil mechanics, to occur when dense, and also loose, granular media, subject to compression, reach the same void ratio at large strains independent of the initial density state.[2–6] A "true" steady-state (i.e., observed constant trace of time series measurements of the macroscopic stress) is difficult to achieve experimentally as stress and volume fluctuations, albeit small in amplitude, are still present.[7,8] This failure to reach an asymptotic steady-state behavior is often attributed to the process of particle breakage, or comminution. However, discrete element simulations (DEM) without modeling a breakage mechanism also exhibit fluctuations in bulk time series in the high strain limit.[6] Due to system size (i.e., number of virtual grains in a DEM) the fluctuations are typically more pronounced than observed in the laboratory.[7] We take the view in concert with others[3,9] that these fluctuations in the stress are a result of dynamical instabilities at critical state; and indeed, the rise and fall of the macroscopic stress, reminiscent of stick-slip motion, is a reasonable analogue to earthquake dynamics in fully developed fault gouges.[10] With this potential and profound application in mind we examine the critical state, or large strain behavior, of macroscopic stress fluctuations in a representative DEM simulation from a nonlinear dynamics and complex systems perspective. This study is undertaken as a prelude to a broader program, aimed towards the development of dynamical systems tools for characterization of the dynamics of geological failure and seismic phenomena, from the length scales of grains to tectonic plates.

Our primarily interest is dense media and this large strain regime. Initially dense samples often evolve in the presence of fully developed shear bands: narrow zones of

a)Electronic mail: michael.small@uwa.edu.au.

intense shear, measuring around ten particle diameters in thickness. Processes inside shear bands are highly dissipative and marked by the birth-death dynamics of force chains. This is in distinct contrast to the essentially elastic loading/unloading cycles observed from the undeforming regions outside, wherein grains move together in almost rigid body motion. The extreme prevalence of shear bands, as a mode of failure in many forms of granular materials, mean that a proper understanding of processes inside shear bands, and associated phenomena such as the aforementioned stick-slip behavior,[10–12] is crucial for the prediction and control of many industrial, civil engineering and geophysical processes. Indeed, so important are shear band dynamics to experimental observations and explanations of critical state behavior that Mooney *et al.*[7] have stated: *"Critical state concepts as applied to ultimate state behavior are applicable only within the shear band, the area that undergoes continued deformation."*

In this study, we examine time series data for the stress ratio, obtained from a simulation of an assembly of polydisperse spherical particles, subject to a biaxial loading condition while particles are constrained to move along a plane. This sample behavior is representative of the behavior in so-called critical state as reported by others (e.g., Refs. 3, 6, 9, 13). In numerical simulations where system size, in terms of number of particles, is generally smaller than in the equivalent soil mechanics laboratory tests, the stress fluctuations or stick-slip become more pronounced and revealing of the underpinning dynamics.

Realistic DEM simulations have the advantage that information at the particle scale is available (e.g., data on particle positions, displacements, rotations, contact forces etc.), facilitating particular details of the microstructural processes responsible for the observed time series, including those governing the rises versus the falls in stress, to be unravelled. Knowledge of these microstructural processes have led to understanding of critical state behavior through characterization of the fabric, contact anisotropy and also predictive models based on micromechanical considerations.[2–5,9,14] More recently, formalisms within the framework of Cosserat or micropolar continuum have combined the strengths of phenomenology and micromechanics to generate a set of constitutive relations valid for this large-strain regime.[15] For samples undergoing localized failure, see also the related local constitutive models developed by Luding and co-workers[16,17] based on observations from two dimensional discrete element simulated compression tests. In particular, a set of differential equations has been formulated by Tordesillas *et al.*[15] from phenomenological relations among the stresses; though phenomenological, the particular form of these relations was inspired from a micromechanical analysis of mechanisms governing fully developed shear bands in the large-strain critical state regime. System dynamics from this model, and anticipated future versions from a purely micromechanical approach, can be characterized using dynamical systems theory, following past models (e.g., Ref. 15). To the best of our knowledge, however, there has been no attempt to extract information on the system dynamics, from a direct analysis of the time series data using either simulation or experimental data. Of interest is whether or not the dynamics as observed from the time series are consistent with the dynamics predicted by the various constitutive models proposed for the large strain critical state regime.

Here, we attempt to bridge this gap through a statistical study, using recent advances in nonlinear time series and complex network analysis, to provide useful information to the continuum modeler, based on the observed rheological behavior from time series of a representative biaxial compression test of a granular assembly. To characterize the physical behavior of this process, we treat the observed data (actually a bulk measurement of Stress Ratio vs. Axial Strain where strain is being increased linearly over time) as a time series. As the level of strain increases beyond the point where the stress ratio reaches a peak and the sample fails through the formation of a persistent shear band, the system approaches a critical state where for further increases in strain, the system dynamical state is approximately stationary. It is the behavior of the system in this post-failure large strain near steady-state regime that is of interest in this paper.

We treat that behavior as a single time series output of a stationary dynamical system and attempt to characterize the dynamics of that system. We note that, in this instance, we consider autonomous system models, and thus axial strain, our proxy for time, is not explicitly used within the models—only the sequential ordering of the stress ratio at observed strains is important. Thus our methods could equally well apply to other loading programs including cyclic shear.[18,19] To achieve this, we use an ensemble of tools which have been available separately, but we combine them to better address a basic problem with black-box modeling. While it is possible to build a model from a time series and then study the behavior of the model, this may not necessarily translate back to the underlying system which generated the data: different models may have different behavior. To better calibrate the models to the data, we apply a range of nonlinear statistical measures to the output of the model and compare this to the data. Once we find a model which has behavior consistent with the data, we are then able to make a much stronger statement about what behavior is being observed in this data. In this case, we find that models consistent with the data—the dynamical instabilities at critical state manifest as fluctuations of the macroscopic stress ratio—exhibit a transient form of chaos.

A. Modeling data and inferring dynamics

Oftentimes, for experimental nonlinear systems, it is not possible to write down a closed-form analytic description of the dynamics. In such situations, it is therefore appealing to apply the methods of delay reconstruction[21] and nonlinear modeling[22] to estimate the underlying evolution operator. One can then use this estimate to study properties of the dynamical system which it represents, and then extrapolate this to the experimental system of interest. Unfortunately, this second step can be problematic. For example, Maquet and co-workers[23] construct global nonlinear models fitted to the Canadian Lynx time series to demonstrate that the data are potentially consistent with chaos: the chaotic dynamics of

the models is claimed as direct evidence of chaos in a real ecosystem. Small and Carmeli[24] reexamined the same data set with their own global models. While these models also—on occasion—exhibit chaotic dynamics, such behavior is far from ubiquitous. In Fig. 1, we plot the original data used by both Refs. 23 and 24 together with an ensemble of model simulations.

For the Canadian lynx data depicted in Fig. 1, model simulations—with the addition of a dynamic noise term—all appear qualitatively to behave very similarly to the observed time series. However, when the models are iterated without noise over a time span far greater than the original data, both chaotic and periodic dynamics are observed with apparently similar frequency. Later in this paper, we will show how this can be more rigorously quantified. However, a second question now arises: given an ensemble of models built from the same data set, which model is correct? This paper will provide a methodological approach to address this problem—although, of course, the question is too ill-posed to allow for a generic answer. For the Canadian lynx data, the answer unfortunately turns out to be that the situation is particularly unclear. The original data simply is not long enough to distinguish between models which exhibit chaotic dynamics from those which are periodic, or, indeed models with an extremely long chaotic transient leading to a fixed point.

B. Dynamical behavior in granular assembles

Nonetheless, the main focus of this paper is to examine a separate, and perhaps more apposite, system. A granular assembly which is compressed in the axial direction at a constant rate (displacement-controlled) and confined laterally under constant pressure, ultimately reaches a near-steady so-called "critical state" regime, in which the bulk stress, measured through the stress ratio, fluctuates about a near constant value.[3,5,6,13,25]

In discrete element simulations and experiments on initially homogeneous and dense granular materials (e.g., sand), these episodic fluctuations in the global stress (also known as stick-slip) often coincide with the presence of fully-developed, persistent shear bands of around 8–10 mean particle diameters in thickness.[25] It is possible for critical state to be approached without localization but here we focus on the dynamics exhibited by a sample which does fail by localization. When failure occurs through strain localization, the spatio-temporal averaged behavior of the material inside the fully developed shear band becomes almost invariant. As Mooney *et al.*[7] pointed out, and Desrues and Viggiani[8] reiterated, critical state can only be reached *inside* shear bands if at all.

Recent studies show that the nature of these fluctuations is intimately tied to the "birth-death" dynamics associated with the growth and failure by buckling of major load-bearing force chains and attendant particle rearrangements inside shear bands.[25–27] An alternative proposal which, under certain circumstance, may provide a not entirely inconsistent explanation of the origins of critical state and localized failure has been proposed by Mesarovic *et al.*[4] through the mechanism of so-called flips. These involve a plastic deformation followed by an elastic relaxation at the particle scale and the authors tie the origin of shear bands to a slight increase in the frequency of these events. However, force

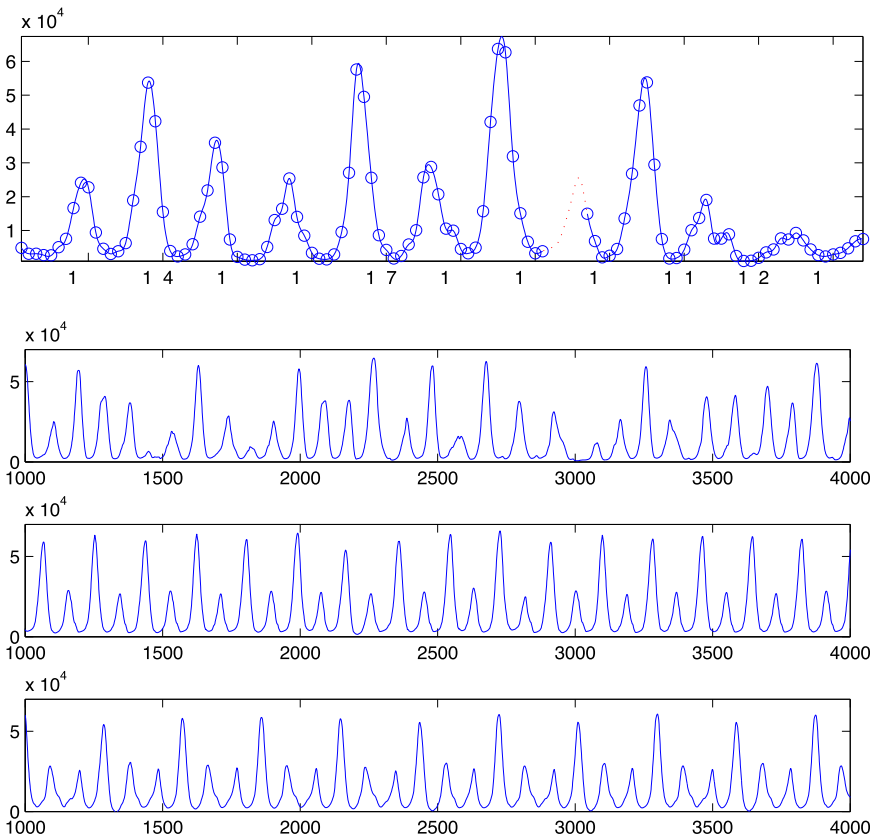

FIG. 1. **The Canadian Lynx time series: chaotic or periodic?** The upper panel shows the original data (open circles) from which various global nonlinear models have been built. The lower panel depicts the dynamical behavior of three such models. The horizontal axis in the upper panel is the observation year: one data point per year. In the lower three panels the horizontal axis are in units of model time steps: 10 time steps per year. Hence, the upper panel covers a period of 115 years, the lower panels cover a period of 300 years. The vertical scales are arbitrary (derived from the total quantity of lynx pelts harvested in a given year). The dynamics observed in the lower three panels are: chaotic, almost periodic and exactly periodic.

chain bucking (emerging at the onset of failure and localized within shear banding) is clearly the dominant micromechanical process to characterize and model—both in order to study the dynamics and physics of critical state behavior in detail as well as the macroscale behavior of geomaterials. Our aim is to use tools from complex systems applied to bulk measurements to help characterize the global behavior of the emergent dynamics resulting from this underpinning mesoscale process.

The outline of the remainder of this paper is as follows: In Sec. II, we describe the representative DEM sample and observed data in more detail. In Secs. III and IV, we summarize our calculations and results. Section V provides a short conclusion.

II. DEM BIAXIAL COMPRESSION TEST

The observed time series, we study is taken from a representative discrete element (DEM) simulation, undertaken to study the rheological response of assemblies of spherical particles, constrained to move in a plane, subject to biaxial compression.[25,28,29] For the sake of clarity and conciseness, we restrict our attention to a single time series. Nonetheless, the methods are completely generic and should be applicable elsewhere. The particular time series we have chosen is a robust representation of dense granular behavior and has already been studied extensively.[25,28–31]

Contact laws, modeling interaction between particles and between particles and walls, describe resistance to relative motion through a combination of linear springs, dashpots, and frictional sliders. Normal and tangential resistive forces, as well as a moment (rolling resistance), act at each contact, in accordance with.[30] The contact moment is introduced to account for the effect of particle shape (e.g., resistance to relative rotations due to particle interlocking[31]). This modification to the classical DEM model of Cundall and Strack[32] has been adopted in numerous simulations of granular processes in order to control the relative rotations of particles at contacts and achieve more realistic rotations and stress predictions (e.g., Ref. 10). Table I provides a summary of the simulation and material parameters used. The vertical side-walls are frictionless, so that particles can slide and roll along them without any resistance; otherwise, all other material properties are identical to those of the particles. The top and bottom walls are assumed to have the same material properties as the particles.

The sample exhibits three distinct regimes of deformation from an initially isotropic state. With respect to Fig. 2, we first observe a period of strain-hardening which can be further identified with two distinct response behaviors. At first, there is a relatively rapid rise in the stress ratio while the sample undergoes a volumetric contraction, up to around $\epsilon_{yy} = 0.02$ at which point volumetric strain reaches a minimum. Second, the sample undergoes dilatation, lowering the rate of increase in the stress ratio compared to the preceding phase before a peak value is reached at around $\epsilon_{yy} = 0.034$. After peak, the second regime can be observed, characterized by a brief period of strain-softening under dilatation. After $\epsilon_{yy} = 0.04$, a pseudo steady-state regime can be observed,

TABLE I. **DEM** 2D biaxial compression test parameters and material properties.

Parameter	Value
Applied strain rate $\dot{\epsilon}_{yy}$	-8×10^{-3}/s
Confining pressure σ_{xx}	7.035×10^{2}N/m
Timestep increment	6.81×10^{-7} s
Initial height:width ratio	1:1
Number of particles	5098
Particle density	2.65×10^{3}kg/m^3
Smallest radius	0.76×10^{-3} m
Largest radius	1.52×10^{-3} m
Average radius (uniform distribution)	1.14×10^{-3} m
Initial packing density	0.858
Interparticle friction μ	0.7
Particle-wall friction μ (top, bottom)	0.7
Particle-wall friction μ (sides)	0.0
Rolling friction μ^r	0.02
Normal spring stiffness k^n	1.05×10^{5}N/m
Tangential spring stiffness k^t	5.25×10^{4}N/m
Rotational spring stiffness k^r	6.835×10^{-2} Nm/rad

whereby stress ratio and volumetric strain essentially taper off to some residual value, modulo fluctuations. This is the region we study here. The deformation in this higher post-peak stress regime occurs in the presence of a single persistent shear band.[25] Stress fluctuations in this steady-state regime reflect the dissipative dynamics in the band; and temporal distributions of micropolar measures of nonaffine deformation have been shown to capture such dissipation.[25] More detailed examination of the spatial and temporal aspects of this dissipation has been tied to the continual formation and collapse by buckling of force chains.[20,25] These discoveries have been used to develop a continuum model of

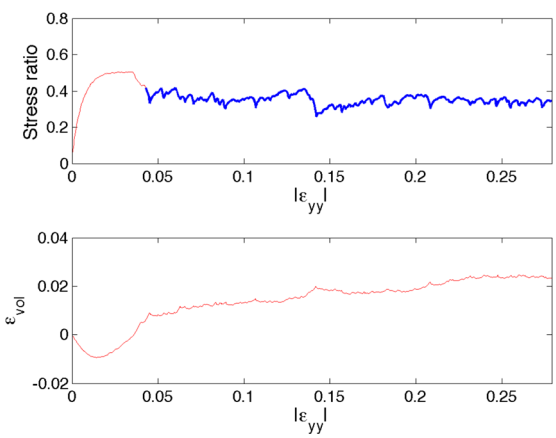

FIG. 2. **Biaxial compression test.** (Top) The observed time series of the bulk measurement of the stress ratio $\frac{\sigma_{11}-\sigma_{22}}{\sigma_{11}+\sigma_{22}}$ with respect to axial strain $|\varepsilon_{yy}|$. The strain interval of interest is indicated by the bolder blue trace and covers the high strain post-peak regime (so-called critical state), where the material has failed and the response is in an approximately steady-state, exhibiting characteristic stick-slip (jamming-unjamming) dynamics. (Bottom) Although not used in the modeling it is informative to soil mechanicians to observe the volumetric strain response ε_{vol} evolution with respect to axial strain. The sample initially contracts and then dilates before reaching a more steady state response in the high strain region from where models in a reconstructed phase space of time-delay stress ratio variables are built.

the stress propagation within a granular material using a Cosserat formalism.[15] A question we seek to answer here is: can a comprehensive black-box modeling approach, encompassing nonlinear time series and complex network methods of analysis applied to bulk measurements, give useful information to help further refine and develop such approaches to continuum modeling?

III. COMPUTATIONS

There are three necessary and distinct steps to characterize the dynamics of an observed time series from noisy experimental observations: (A) reconstructing the phase space, (B) estimating the evolution operator, and (C) verifying that the model behavior matches the observed data. Each of these steps can be achieved with a host of methods, and which methods one chooses depends on the proclivities of the practitioner. While the choices we make are personal and based on our own bias, rather than necessarily optimal, they are nonetheless well established. Much of this background can be found in several texts and monographs; we recommend Small[22] for obvious reasons.

Our approach, described in detail below, combines tasks (A) and (B) above. Before proceeding, however, we find it useful to follow the more standard application of the nonlinear time series toolbox for reconstructing a phase space to analyze the time series to gain insights into the character of the underlying dynamics.[33] The methods of nonlinear reconstruction are built on the assumption that the underlying dynamical system explaining the process can be represented by a set of ordinary differential equations whose state space has dimension d. Since, we typically only have access to a scalar time series—in our case the observed macroscopic stress ratio—which is some projection of the d-dimensional state variables, we must reconstruct an equivalent phase space to help characterize and model the dynamics. This can be achieved subject to some general conditions by the method of time-delay embedding[21] whereby a coordinate system of dimension d_e—the embedding dimension—is constructed by using values of the time series and its delays at a given lag. We want trajectories in this reconstructed phase space to smoothly unfold the dynamics so that points close within d_e-dimensional space will evolve together over short time intervals. Thus d_e must be selected large enough so that the geometry of points close to each other are close to each other due to the dynamics and not because of a poor projection to too low a dimension.

Typically, $d_e > d$ and one approach for determining a useful value for d_e is the method of false nearest neighbors.[33] For a given lag, the time series is embedded in successively higher dimensions and the percentage of false neighbors (i.e., the proportion of points close together due to projection rather than dynamics) is calculated. The value of d_e when this percentage falls to zero or a noise floor is regarded as a good choice of global embedding dimension. Computation of the proportion of false nearest neighbors observed for increasing embedding dimension (here, embedding lag set to 1) is shown in Fig. 3 along with computation of local false nearest neighbors.[34]

Local false nearest neighbors is a modification of the method of false nearest neighbors which takes a prediction horizon of the dynamics into account as well as the geometry of phase space. Local false nearest neighbors is capable of detecting the true dimension of the underlying dynamics (d_L) or the number of active degrees of freedom in the system. We have $d_L \leq d_e$. False nearest neighbors indicates a global embedding dimension of $d_e = 6$ while local false nearest neighbors indicates that the local dynamics can be embedded in $d_L = 4$ dimensions—hence at least a four dimensional

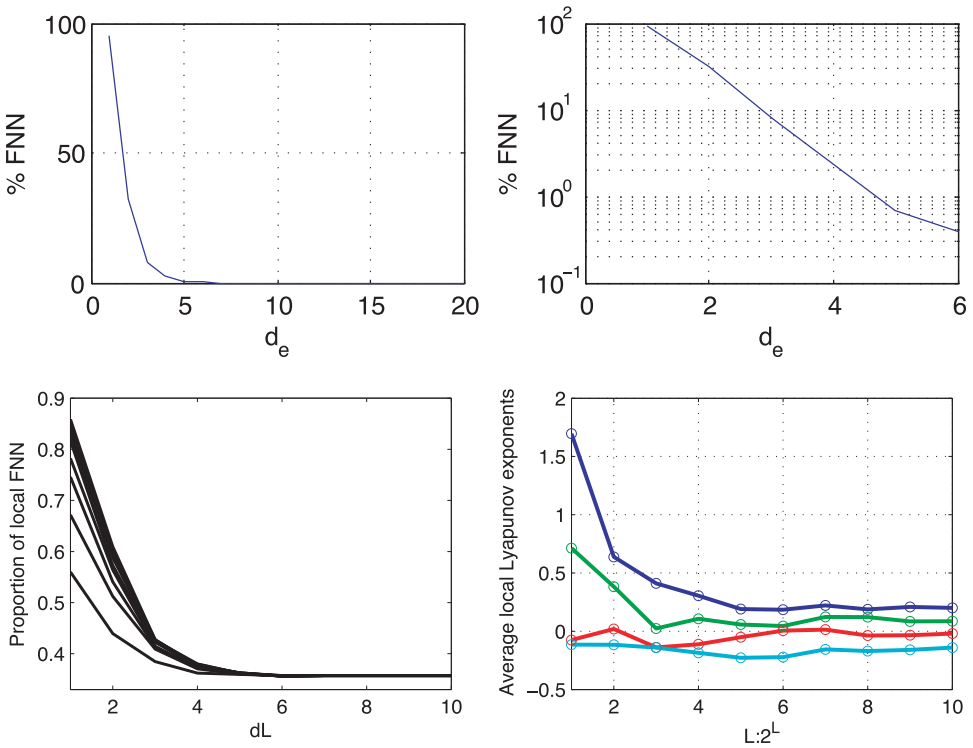

FIG. 3. **False nearest neighbors.** The upper two panels depict the proportion of false nearest neighbors (embedding lag 1) for the data depicted in Fig. 2. For $d_e > 6$ there are no false nearest neighbors, the proportion drops to almost 0 for $d_e > 4$. The lower panel is the proportion of local false nearest neighbors, a measure of the locally sufficient embedding dimension, for local dimension $d_L \leq d_e = 6$ (again, embedding lag is 1 and the prediction horizon is 3). The calculation is repeated for various n = local neighborhood sizes $N_b = 10, 20, 30, \ldots, 100$ and plateau onset at a local dimension of $d_L = 4$ is evident. The local Lyapunov exponent spectrum indicated four genuine exponents with one or two positive.

system of ordinary differential equations is required to describe this system, i.e., four state variables. This is consistent with isostatic Cosserat continuum formalisms to model stress and strain relationships.[15]

Having established a suitable global embedding dimension and obtained knowledge of the number of active degrees of freedom in the system, we can go a step further and reconstruct local models of the dynamics. These models can take the form of linear or quadratic maps which approximate the evolution law of reconstructed phase space points based on the observed dynamics of nearby reconstructed phase space points. We can extract the Jacobian matrices of these local models and combine them to calculate the local Lyapunov exponent spectrum over strands of length $2^L, L = 1, 2, \ldots, L_{\max}$.[33,35] The Lyapunov exponents are dynamical invariants and their signs help to characterize a dynamical system. If the underlying dynamics is represented by an ordinary differential equation, one of the exponents will be zero. A chaotic system has one positive Lyapunov exponent and if a system has two or more positive Lyapunov exponents, it is termed hyper-chaotic. Moreover, for dissipative systems the total sum of Lyapunov exponents is negative. Computation of the Lyapunov exponent spectrum using local linear maps with $d_e = 6$ and lag 1 is shown in Fig. 3. We find four genuine exponents consistent with $d_L = 4$ and the sign distribution of the exponents is seen to be $++0-$ or $+0--$ depending on which of the close to zero exponents is chosen as the zero exponent.

The above first steps of application of the nonlinear time series toolbox has shown that the number of active degrees of freedom of the underlying system as determined by analyzing the observed time series is four. The local Lyapunov spectrum is consistent with this identification; however, whether or not the process is best described by a nonlinear chaotic or hyper-chaotic system is unclear given the accuracy of the approximation to the exponents. Given these insights and uncertainties, we now depart from the conventional approach and describe our method of embedding (A), modeling (B), and testing (C) in order to further characterize the dynamics based on the observed data.

A. Embedding

We start with an observed scalar time series $\{x_t\}_t$—here, the observed macroscopic stress ratio. Generically, we assume that the underlying system has dimension d and to reconstruct it one must choose an embedding dimension $d_e > d$. Following Refs. 36 and 37, we do not concern ourselves with the appropriate choice of embedding lag, but leave that to the modeling algorithm. Rather, we choose $d_e \gg d$ such that the vector variable v_t can now be treated as an over representation of underlying deterministic phase space

$$v_t = (x_t, x_{t-1}, x_{t-2}, x_{t-3}, \ldots x_{t-(d_e-1)}). \tag{1}$$

Thus v_t consists of observed values of the stress ratio and its time delays (i.e., past values).

B. Modeling

The second step is to estimate the evolution operator. That is, the law which maps the reconstructed phase space of stress ratio at time t (i.e., v_t) to the next reconstructed data point at time $t+1$ (i.e., v_{t+1}). In general this is the closed-form expression diffeomorphic to the dynamic evolution of the underlying system and is a map from $\mathbf{R}^{d_e}$ to $\mathbf{R}^{d_e}$. For us, Eq. (1) makes the task a little easier, and we instead seek a function $F : \mathbf{R}^{d_e} \to \mathbf{R}$ such that

$$F(v_t) = x_{t+1}, \tag{2}$$

and hence $v_{t+1} = (F(v_t), x_t, x_{t-1}, \ldots x_{t-(d_e-2)})$. Of course, there are many choices for algorithms to estimate F. The one we choose was first described by Judd and Mees[38] and more recently extended by Small and co-workers.[39,40] In summary, this approach constructs a function F of the form

$$F(v_t) = \lambda_0 + \sum_{i=1}^{b_1} \lambda_i v_{t-\ell_i} + \sum_{i=1}^{b_2} \lambda_{i+b_1} \phi\left(\frac{|v_t - c_i|}{r_i}\right), \tag{3}$$

where the weights λ_i are chosen as the best linear fit; the nonlinear terms ℓ_i, c_i, and r_i are chosen with a nonlinear algorithm combining stochastic search and local steepest decent optimization; and, the model size terms b_1 and b_2 are constrained using the minimum description length criteria of Rissanen,[41] as outlined in Judd and Mees.[38] The functions $\phi(\cdot)$ are chosen to be functions of a single variable defined on $[0, \infty)$: Gaussian $(e^{-\frac{x^2}{2}})$, cubics (x^3), Morlet wavelets $(\cos(2\pi\frac{x}{s})\exp(-2(\frac{\pi}{5})^2(\frac{x}{s})^2) - \exp(-\frac{5^2}{2} - 2(\frac{\pi}{5})^2(\frac{x}{s})^2))$ or sigmoids $(\tanh\frac{x}{s})$. Note that we have relaxed the usual requirement of compact support frequently associated with radial basis functions (in our experience doing so actually increases the flexibility and stability of our models—at the expense of analytic tractability) and allow for a variety of different basis functions within a single model: in effect, the term $\phi(\cdot)$ in Eq. (3) should more properly be written as $\phi_i(\cdot)$ and it is understood that each such function is one of the forms listed above. Finally, some of these functions ϕ_i (the wavelets and sigmoids) include a second nonlinear parameter s—when such is needed this second parameter is fitted following the same procedure as described above for the basis radius terms r_i.

Now that we have described the model, it is clear that there is no possibility of a computationally tractable algorithm to provide the global optimum. Nor, indeed, would it necessarily be very good: it is quite likely that such an optimum may exhibit rather sensitive dependence of the various model parameters. Instead, we utilized a variety of stochastic and heuristic search algorithms to generate good models of the observed data. From these models it is easy to generate simulations of the underlying dynamics via a modified version of Eq. (2)

$$x_{t+1} = F(v_t) + e_t, \tag{4}$$

where $e_t \sim N(0, \sigma^2)$ is some Gaussian distributed noise term of fixed variance σ^2. The assumption of additive Gaussian noise is reasonable here because the linear fit of the parameters λ_i as well as the computation of minimum description length both employ it. The noise variance σ^2 will be some fraction of the total mean-square error of the model fit to the

data: one assumes that the model prediction error is composed both of dynamic and observation noise.

It should be clear that this model class is rather generic. In particular, by fitting a model of the form (3) we are not imposing any *a priori* dynamics on the system—the model just seeks the simplest description of the one-step prediction problem (2). Our task for the remainder of this paper is twofold: (i) to validate the model performance (i.e., which models do a good job of matching the system dynamics) and (ii) classifying the model dynamics (exactly what dynamical properties do these models have). To do this, we generate an ensemble of model simulations and study these data. What we will find is, despite the extremely broad scope offered by (3), models fitted to the DEM data exhibits a fairly narrow range of behaviors.

With these simulations in-hand, the next step is to determine which simulations, and therefore which model(s), most closely matches the observed data. That is, we have obtained a suite of black-box models which predict the future values of stress ratio given information of past and current values of stress ratio. Each model will have captured the dynamics to a greater or lesser extent and we now identify through extensive testing and comparison with the observed stress ratio data which models have captured the salient character of the underlying system dynamics best.

C. Model testing

It is an element of faith, particularly within the machine learning and artificial intelligence communities, that the model with the smallest prediction error when tested on previously unseen data is necessarily the best model. However, we are interested in the dynamic behavior of the system and this is simply not necessarily the case.[42,43] Instead, we follow the approach implied by the surrogate data methods for statistical hypothesis testing.[44] Surrogate data methods provide a computational method to determine whether an observed time series is consistent with a particular null hypothesis (linearly filtered noise, for example). To achieve this, one generates an ensemble of time series that are similar to the observed data but also consistent with the null hypothesis (in this case of linearly filtered noise, this is done by randomizing the phases of the Fourier transform of the data[45]). There is no reason not to apply the same philosophy here to

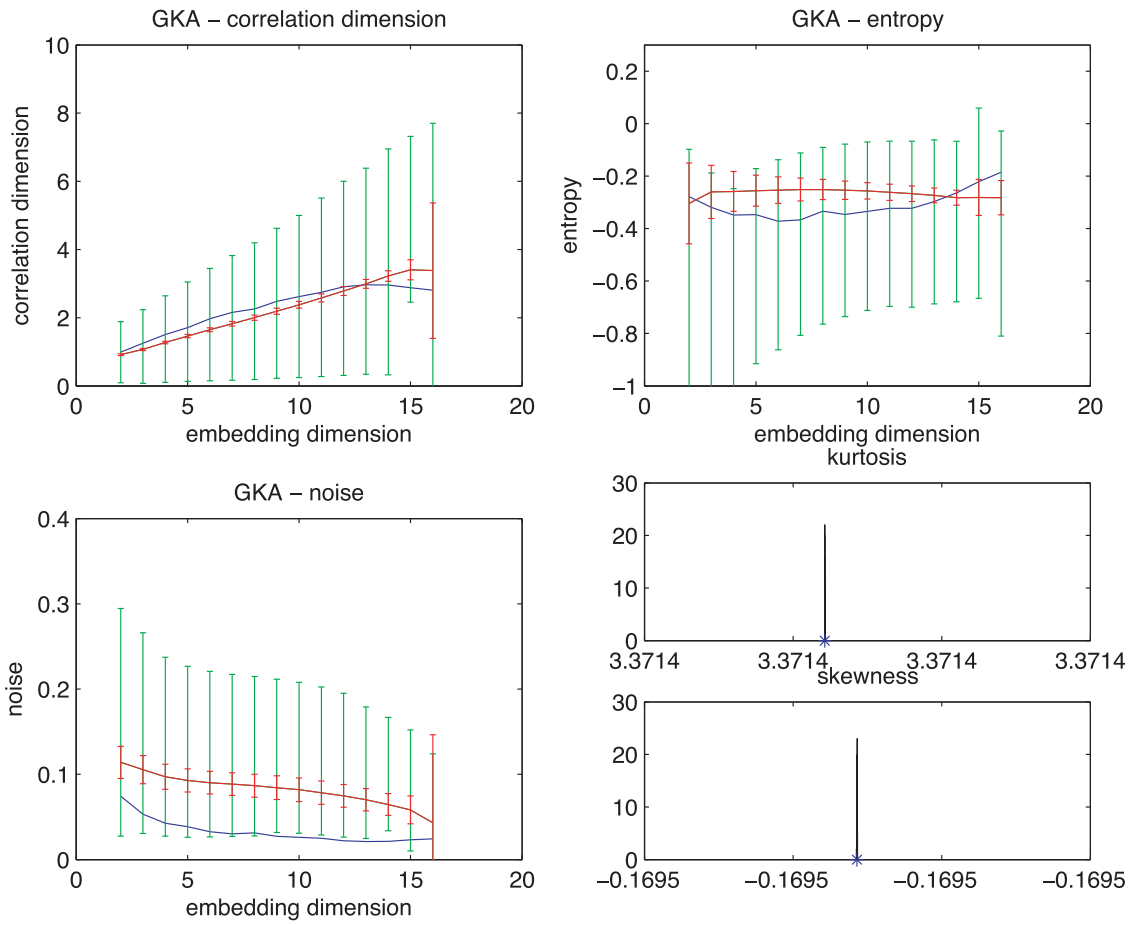

FIG. 4. **Linearly filtered noise.** Comparison of nonlinear statistics computed with the Gaussian Kernel algorithm (correlation dimension, entropy and noise level), and higher order linear distribution statistics (skewness and kurtosis), for the original data in Fig. 2 and linear surrogates (monotonic nonlinear transformations of linearly filtered noise). As expected the linear statistics (lower right plots) show no difference. However, the nonlinear measures indicate that the linear model does not adequately described the dynamics (upper panels and lower left). For the nonlinear measures, the solid blue lines (no error bars) indicate the statistic values computed for the data (as a function of the embedding dimension—a parameter of the statistic). The tight error bars (red) are the mean and standard deviation from 100 simulations, the larger error bars (green) are the full range (minimum to maximum). For the higher order linear statistics, a distribution of values is plotted, the value for the data are indicated as an asterisk.

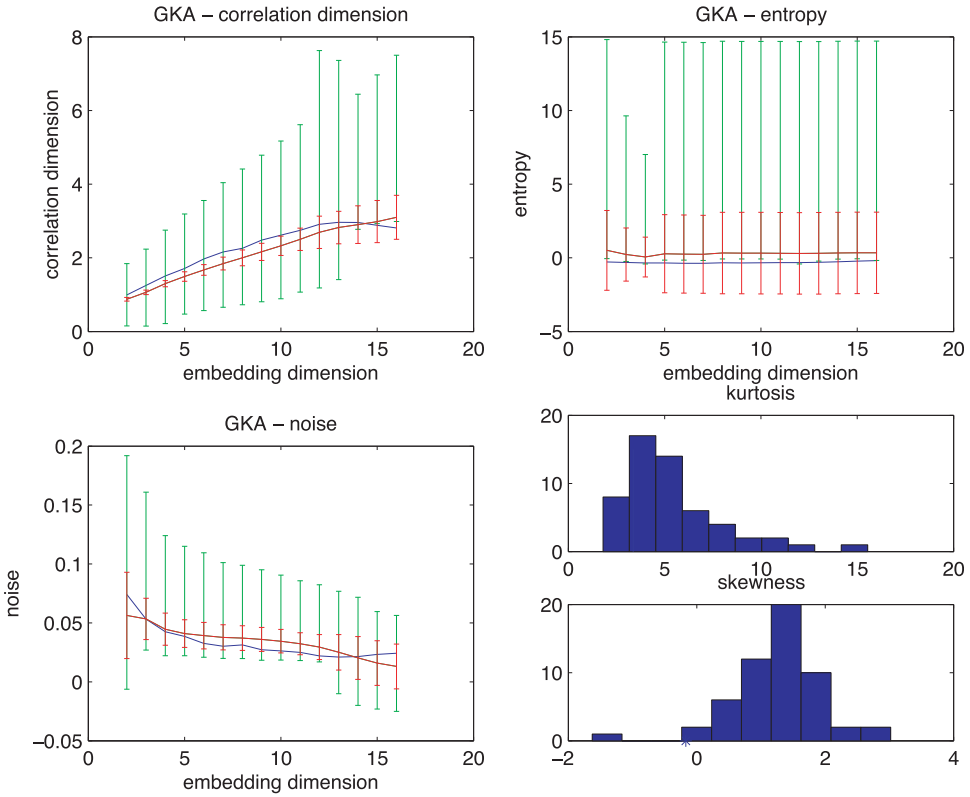

FIG. 5. **Stable node.** The data displayed here are in the same format as Fig. 4, except here the 100 simulations come from a model of the data driven by noise. In the absence of noise the model exhibits a stable node.

test whether a given model is consistent with the observed time series data. Since we are interested in the dynamics of the simulation, we wish to compute measures relevant to the dynamical system. Small and Judd[44] demonstrated that correlation dimension is a suitable statistic for such a task—at least for specific types of models. In this paper, we employ a larger battery of statistics with the aim of addressing a more general range of problems: we wish to find the models that match the data well.

In the following, we employ a number of statistics to compare the model behavior to the original data. Lack of space prohibits all but a cursory description of each measure.

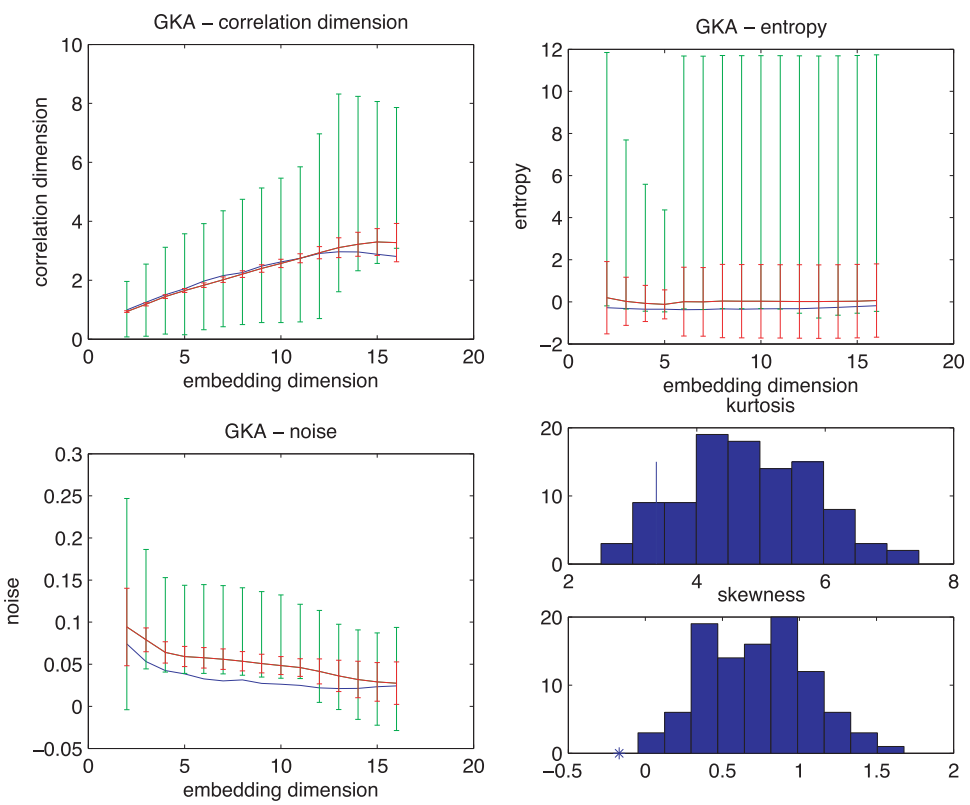

FIG. 6. **Stable focus.** The data displayed here are in the same format as Fig. 4, except here the 100 simulations come from a model of the data driven by noise. In the absence of noise the model exhibits a stable focus.

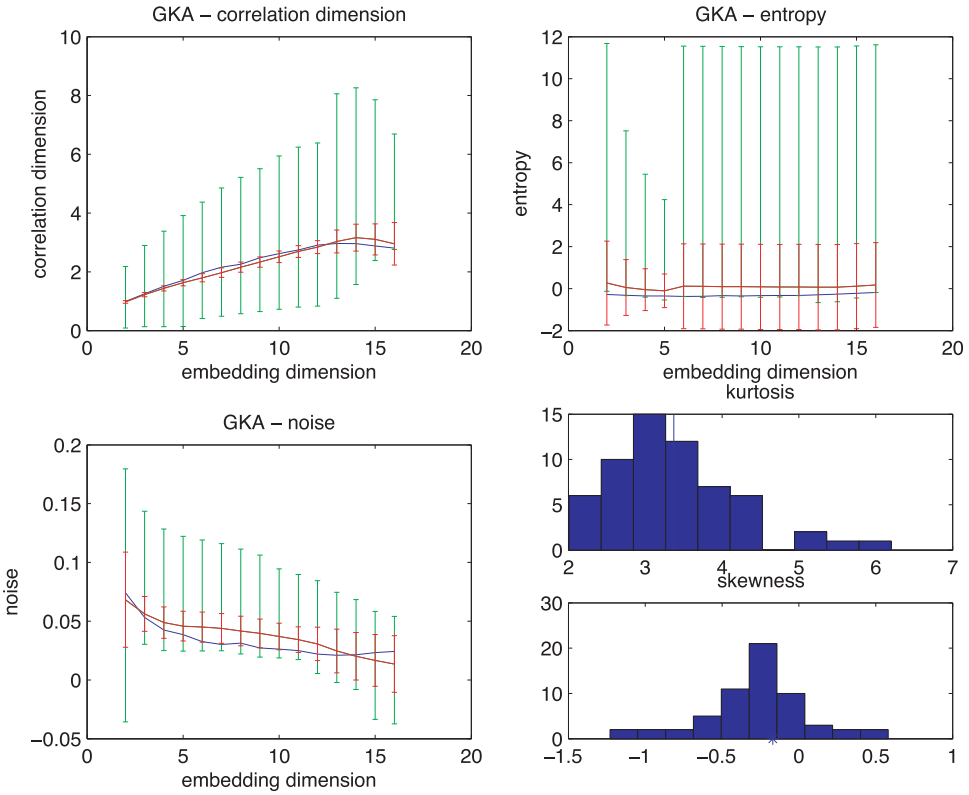

FIG. 7. **Transient chaos.** The data displayed here are in the same format as Fig. 4, except here the 100 simulations come from a model of the data driven by noise. In the absence of noise the model exhibits a chaotic transient (typically over a time scale longer than the observed data) and a stable fixed point.

Skewness: A linear measure of asymmetry in the probability distribution of the observed data. Skewness is defined as the standardized third moment of a random variable X of mean μ and variance σ^2 : $E\left[\left(\frac{X-\mu}{\sigma}\right)^3\right]$.

Kurtosis: Likewise, kurtosis is the standardized fourth moment $E\left[\left(\frac{X-\mu}{\sigma}\right)^4\right]$ and is a measure of peakiness of the probability distribution.

Correlation dimension: The Gaussian kernel algorithm[46,47] (GKA) is used as a robust estimate of correlation dimension for a range of embedding dimensions. The correlation dimension measures the structural complexity of the underlying deterministic attractor.

Entropy: Also estimated by the GKA, the entropy is a measure of the rate of novel information generation in the system.

Noise: Intrinsic to the estimation of the deterministic dynamics in the system, provided by the GKA, is an estimate of stochastic (observational) noise.

TABLE II. **Complex network statistics.** For the original data and each of the three model classes, we computed observed values of the various complex network statistics: mean path-length (aka diameter), clustering, and assortativity. In each case, the mean value and standard deviation are reported. Also reported is the number of simulations (out of 100 attempts) which remained bounded. According to these measures both transient chaos and stable node dynamics are in agreement for two out of the three measures and differ marginally for the third.

Model	N	Diameter	Clustering	Assortativity
Data		13.1	0.353	−0.122
Stable node	58	16.0 ± 2.7	0.360 ± 0.0251	−0.079 ± 0.060
Stable focus	100	12.1 ± 0.88	0.388 ± 0.0146	−0.0084 ± 0.053
Transient chaos	77	13.1 ± 0.84	0.358 ± 0.0172	−0.053 ± 0.058

Motif distribution: In addition to the standard nonlinear time series measures described above, we transform the data into a complex network and compute several properties of the complex network. Following Ref. 48, we compute the motif superfamily distribution of the network representation. We focus on motifs of size four (connected subgraphs of

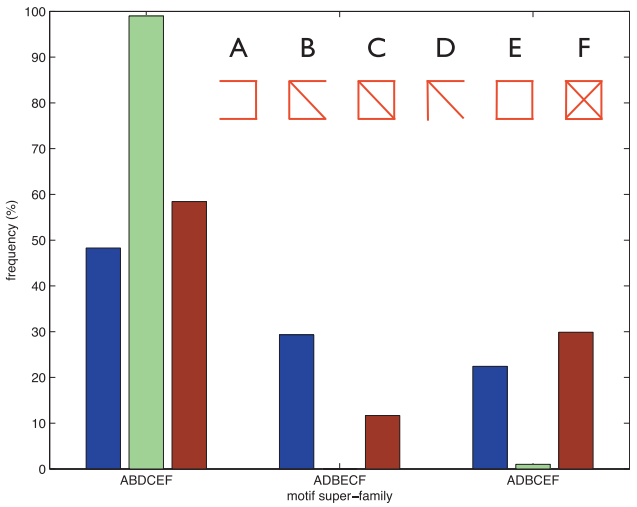

FIG. 8. **Motif frequency figure.** For each of the three model dynamics we computed the motif super-family which occurred most frequently—shown here as a percentage. Motif family ADBCEF is the corresponding family for the data (the right-most batch of columns). In models exhibiting a stable focus, for example Motif ABDCEF occurred for all but one of the model simulations, that exception was ADBCEF. According to this measure, stable node and transient chaos models exhibited behavior most similar to the data. *Inset*: the structure of the six four node motifs. The motif-superfamily is a ranking by frequency of sub-graphs of order 4. The inset enumerates the six different motifs of order 4 which are possible. The horizontal axes of the upper panel is a ranking of these six classes (from most frequent to least).

four nodes) and compute the relative frequency of the distinct graphs, up to node permutation.

Mean path-length: We also compute the mean path-length, defined as the expected minimum distance between two random nodes within the network giant component[49]—confusingly, also referred to as **diameter**.[50]

Clustering: Also computed from the network representation, the clustering coefficient is a measure of the frequency of occurrence of fully connected motifs of size 3 (triangles) within the network.[50]

Assortativity: The final network based measure we compute is assortativity. Assortativity is a measure of the propensity for connected nodes to have similar properties. In this case, the property we are interested in is degree. The measure of similarity is the linear correlation coefficient of linked nodes—that is, how well the degree of one node (linearly) predicts the degree of its neighbors.[50]

The linear statistics, skewness and kurtosis, are nothing more than a measure of the distribution of the observed data values: there is no temporal information encoded in these numbers. Nonetheless, they provide a good test of the fool-proof-ness of our algorithm: the model of dynamics should at the very least also replicate the distribution of observed values. Moreover, this is not something which one explicitly requires from the modeling procedure itself and it therefore provides a significant non-trivial and indirect test of dynamical behavior. The nonlinear time series measures (correlation dimension, entropy, and noise level) estimated from the Gaussian Kernel algorithm[46,47] provide a good test of the model's ability to reproduce the dynamical attractor of the system. Finally, the complex network based measures provide direct tests of the form of the underlying dynamics.

IV. RESULTS

Here, we summarize the results for representative models of four different types. In Fig. 4, we employ linear surrogates[45] to generate an ensemble of realizations of a linear noise process which closely resemble the original data.

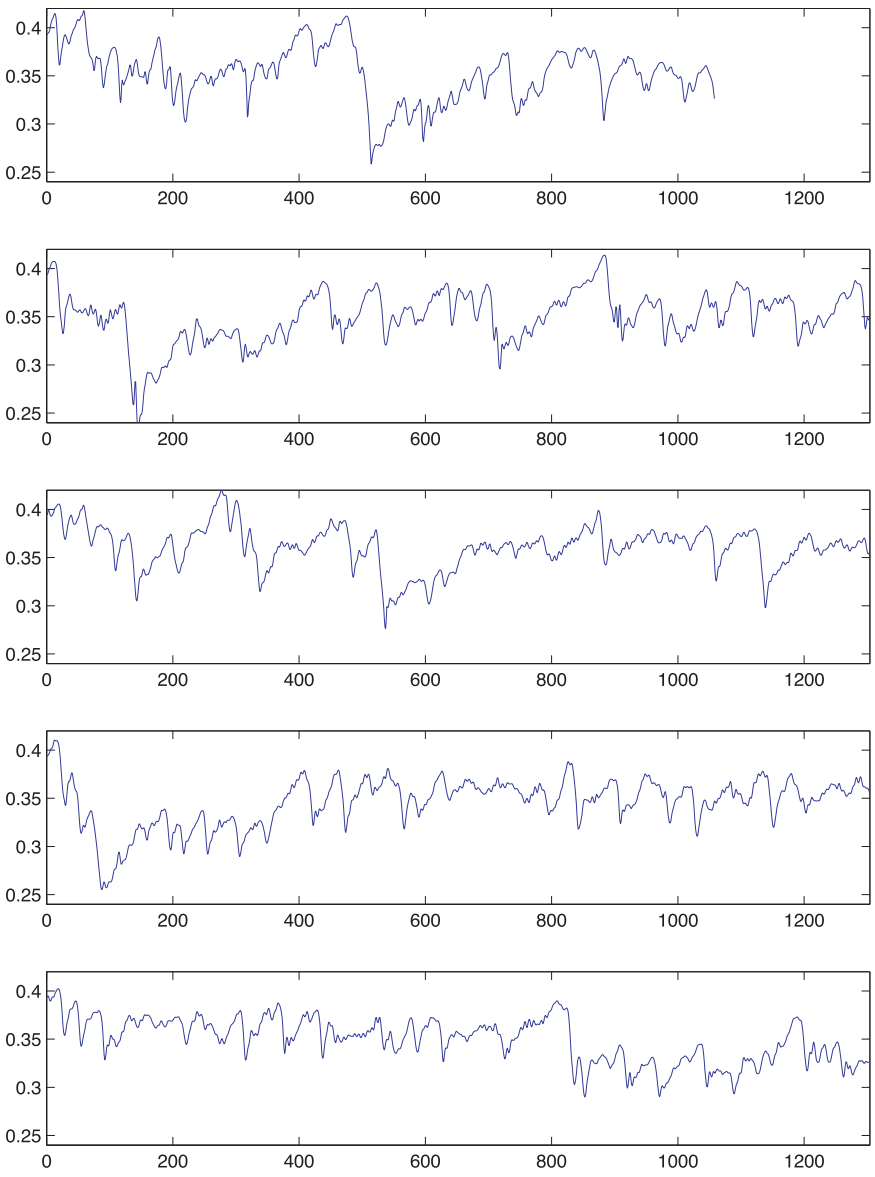

FIG. 9. **Sample trajectories.** The top panel depicts the original data. The following four panels are iterated free run simulations, with dynamical noise for four different simulations from the model exhibiting transient chaos and the same motif super-family as the data.

Nonetheless, Fig. 4 clearly demonstrates that the data and surrogates are distinct. In the next three figures, we test the three distinct classes of nonlinear models which we observe arising from this data.

Figures 5–7 plot a comparison between model simulations and the original data for models exhibiting a stable node, stable focus, or transient chaos. Based on this comparison, we see that transient chaos offers the best match between the model simulations and the data.

In Table II and Fig. 8, we summarize the results from our statistics based on complex networks. These results are consistent with the linear and nonlinear time series measures described above. In Table II, we see that network diameter and clustering show a very close agreement between the model exhibiting transient chaos and the data—that is, the value for the data is typical of the observed distribution for these models. The models exhibiting either a stable node or focus consistently deviate more from the data—while the data are still within two to three standard deviations of the mean observed over the models, it is less typical. Interestingly, measured assortativity does not show such a good agreement for any of these models: in part this is because the models exhibit values of assortatvitiy that are closer to zero than for the data. While, for example, the mean assortativity of the stable node models is within one standard deviation of the value estimated for the data, this distribution is somewhat skewed toward 0. This indicates that assortativity is not only a very sensitive measure of nonlinear dynamical structure in the data, but that we do not yet have the full picture. Nonetheless, the deviation between assortativity for the models and the data are certainly not statistically significant—for both the stable node models and transient chaos the observed value of assortativity for the original data are within 1.5 standard deviations of the mean.

In Fig. 8, we summarize the results from the motif super-family characterization. For each time series (either from the data or a model simulation), we construct a network—it is this network which is used to estimate the properties summarized in Table II. From this network, we compute how frequently each possible subgraph of size four occurs—each subgraph (see, *inset* of Fig. 8) is depicted by a letter and the ranking of their frequency leads to a string such as ADBCEF. Figure 8 provides an indication of which motif super-family (ranking) occurs most frequently. In all cases (either stable node, stable focus or transient chaotic dynamics) the most frequent motif for the models is not the same as the data. However, the second most commonly occurring motif for models with either transient chaos or a stable node is identical to the motif super-family ranking observed for the data. Finally, when we consider only those models with the same super-family as the data, we note that there is a very good agreement in the measured value of assortativity: for transient chaos models with the super-family ADBCEF (the same as the data), the mean value of assortativity is -0.091 ± 0.05. Moreover, simulations from such models are clearly qualitatively similar to the data (Fig. 9). All three motif super-families we report here (ADBCEF, ABDCEF, and ADBECF) are consistent with what was reported previously for deterministic time series contaminated with observational noise.[48] The motif ranking ADBCEF was reported in Ref. 51 as indicative of noise contamination; motif ranking ADBECF occurs from this by very slightly changing the frequency of motif E and C.

Note that the motif super-family ranking is a local measure of dynamical structure in the data: it is a measure of connectivity patterns between similar states in the system state space. The various configurations that are possible (the motifs) are constrained by the local dimension of the underlying dynamics and this, in turn, dictates which motif super-family will arise. Hence, for example, the distinction between chaotic dynamics (or transient chaos or hyper-chaos) and periodic flow or a noisy stable state is a question of what the local embedding dimension of the flow is. Although we arrive at a method capable of distinguishing chaos from noise this method is independent of estimation of the Lyapunov spectrum.

In Fig. 10, we depict the dynamical behavior of this same system in the absence of noise. Note that the dynamics appear to exhibit chaotic dynamics for a very long time (several times longer that the length of the data) before eventually reaching a stable fixed point. The embedded data in Fig. 10 and also Fig. 11 illustrates the high dimensional deterministic dynamics during this phase. In Fig. 11, we also plot a complex network constructed from this data. The network structure evident here is similar to the chaotic and hyper-chaotic systems exhibited in Ref. 49. Moreover, the motif super-family ranking computed for this noise free deterministic system is ABDCEF—the same motif super-family distribution as that reported in Xu *et al.*[48] for hyper-chaotic flow systems.

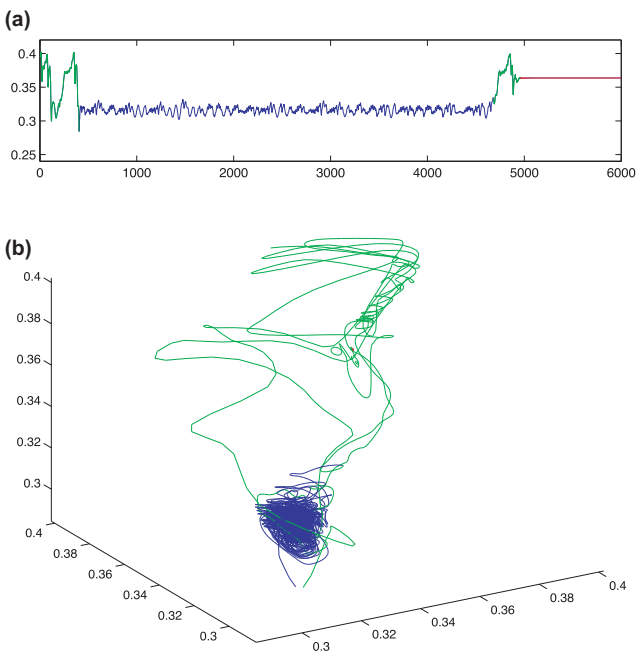

FIG. 10. **Sample trajectory.** The top panel depicts a single noise free simulation exhibiting transient chaos dynamics. The lower panel is an embedding of the same data (color coded to depict different dynamical regimes). Note that the system appears to switch between two different dynamical behaviors before eventually collapsing to a fixed point. The time scale is the same as Fig. 9.

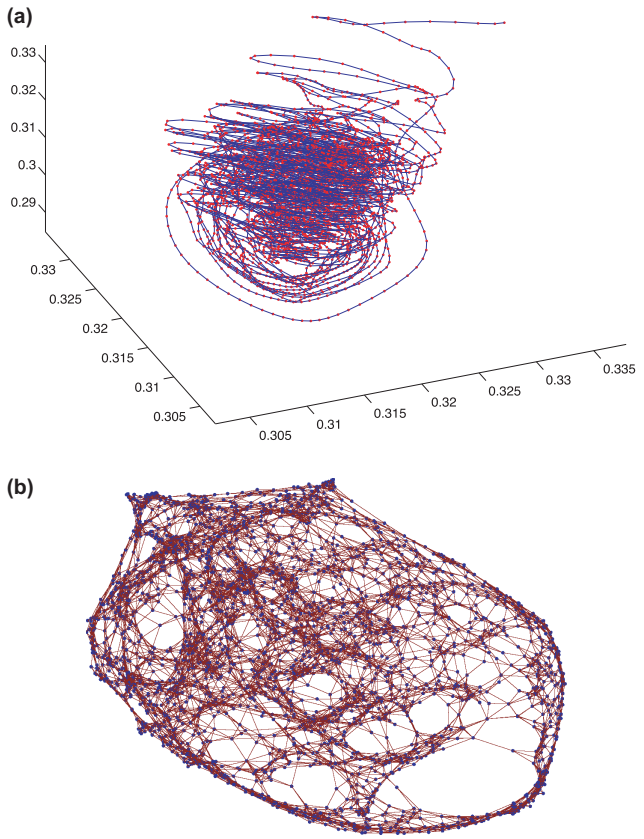

FIG. 11. **Sample trajectory.** The left panel depicts a short section of the embedded data from Fig. 10—the section is representative of the transient chaotic state and is the purely deterministic model output (no noise). On the right is the complex network constructed from this embedding.

V. CONCLUSIONS

While none of the constituent methodologies, we have presented in this paper is entirely new, what we have done is to systematically bring these methods together as a way to describe the dynamics underlying an observed time series. This is something that has been done in an ad hoc manner for some time. Unfortunately, this "ad hockery" often led to results which depended excessively on the particular modeling scheme employed by the investigators. While we too have our favorite modeling methods (and have employed them to infer system dynamics in the past[39,52]), what we have presented here is an approach which is robust against variation in modeling methodologies. The model can only be said to really reflect the underlying dynamics if a battery of independent and demanding statistics demonstrated no significant deviation. For our test case from population dynamics, we were unable to do this and the only conclusion that we could reasonably make was that there was insufficient data.

For the biaxial compression test, with strain in the system acting as a proxy for time our results are more conclusive. Each of our chosen statistics (spanning linear statistics, nonlinear time series analysis and methods from complex network theory) indicated strong agreement between the data and noisy simulations of a system exhibiting a form of transient chaos. While the transient nature of this chaotic dynamics is interesting from a computational perspective, it is probably only a numerical artifact. The transition time often exceeds the length of recorded data, and the system never reaches a stable equilibrium in our simulations because of the addition of dynamical noise. Numerically the results are indistinguishable from true chaotic dynamics with a dynamical noise component. Motif super-family calculations suggest that the dynamics are in fact consistent with hyper-chaos with the addition of a dynamical noise forcing. This is also consistent with our calculated approximation to the Lyapunov spectrum from the observed data containing two positive sign components as well as a determination of the number of active degrees of freedom in the system being four.

In contrast to the population dynamics test case, a further benefit of focusing on the granular system comes when we try to seek a physical explanation of our characterization of the observed dynamics given what has been learned about granular rheology in earlier work. Specifically, we can seek explanations in terms of force chain dynamics. Force chains are columns of particles which align themselves in the direction of maximum (most compressive) principal stress. In recent work, we discussed the underlying mechanisms in the observed fluctuations in global stress.[25] These are corroborated by findings from high resolution experiments on sand,[53,54] which suggest that regions of high (hyperstatic) and low (isostatic/hypostatic) coordination numbers alternate spatially along the band, with the former being jamming zones where force chains grow, and the latter being unjamming zones where force chains collapse by buckling. The relative dominance of these two competing events of jamming and unjamming determines which of the elastic rises and unstable drops in the strain evolution of the macroscopic stress occur. Thus, in the so-called critical state regime wherein the equations of Ref. 15 hold, and for which the sample deforms in the presence of fully developed shear bands, the macroscopic stresses result from both spatial and temporal averaging of the stresses borne by the constituent force chains in the system at varying stages of their respective loading histories. The analysis in Ref. 15 shows that the governing equations for the critical state must embody at least three autonomous state variables in order to capture the dynamics of collective force chain evolution. Recall, the numerical local false nearest neighbors calculation of Fig. 3 which suggests that four degrees of freedom (i.e., four state variables) may be necessary to describe the observed dynamics. Indeed, a minimum of four ordinary differential equations is necessary for hyper-chaotic behavior. Thus, our modeling approach given the observed data suggests that researchers formulating physical laws for dynamics at, or on the edge of, critical state should perhaps only make simplifying assumptions and continuum averaging, to the extent that the number of active degrees of freedom are at least what we expect—to simplify further risks restricting the range of observable behaviour.

Critical state soil mechanics and numerical and experimental evidence[2,3,7,8] suggest that within the shear band the ultimate dynamics of the system for a given material collapse onto a subspace whereby the variables associated with

mean effective stress, deviatoric stress, and specific volume follow a so-called critical state line. That is, from a dynamical systems point of view, there are integrability constraints and constants of the motion relating a system description using these variables. Our black-box modeling and testing methods described here do not explicitly take into account this knowledge but it is a straightforward extension to consider more "grey-box" models that formulate the critical state line as constraints within the model estimation step (B). This is the subject of ongoing research given that the reconstructed state space considered here only uses observed values of stress ratio and does not take advantage of other multivariate measurements. However, the richness of the dynamical instabilities, we have uncovered within our representative sample gives cautionary counsel that an imposition of such a constraint is making the model fit the theory rather than having the model and data inform theoretical development. We are also in the process of extending the analysis to other systems on the edge of critical state as well as to experimental tests of granular shear layers,[12] which have been shown to exhibit stick-slip dynamics similar to those observed in earthquake signatures.

In dense granular materials subject to compression, force chain "dynamics" or evolution inside shear bands dominate the behaviour in the so-called critical state for samples undergoing localised failure. Furthermore shear band widths are almost universal across all types of sand and loading. Thus considering larger and larger number of particles in the system tests should not be an important factor. It is certainly not a factor that seems to affect the macroscopic behavior of the system. More specifically, the birth-death evolution of force chains (i.e., formation and failure) are responsible for the fluctuations observed in this data (the data we present in this manuscript). The death or collapse of force chains for dense media, tends to localize along zones with a characteristic thickness (this width is widely known to lie within a very narrow range of 8–20 particle diameters). This means that even if the material manages to form a force chain that extends by some hundreds of particles in length (a very big sample), the buckling of force chains will still be localized to a region that is roughly 8–20 particles wide.

This feature is observed experimentally for a wide range of dense granular materials, both naturally occurring and synthetic. We already have some answers as to why this may occur in a recent paper using structural mechanics analysis of a column of N particles.[55]

Tordesillas and co-workers[55] studied the confined elastic buckling of a single N-particle force chain. For a given set of material parameters, a characteristic load-carrying capacity is attained for a clearly defined range of force chain lengths $N \geq L^*$. The rotation and translation of particles along periodically located segments of the critical buckling mode, each of length L^* are on average consistent with those for particles inside the shear band. Preliminary results from postbuckling analysis show that the critical buckling mode is unstable and that buckling culminates in a localized response over one of these segments where observed shear band kinematics prevail. Thus, the localized buckling response is characterized by the rotation of a finite number of particles with a clearly defined length L^*. For a wide range of material properties, L^* is around eight particle diameters—the observed shear band thickness for many granular materials, most notably sand.

Hence, although the bulk of this paper focusses on the analysis of a single DEM simulation, the result is actually what we would expect more generally. While that data set is accepted as a robust representation of dense granular behavior, there would be obvious extensions of this work to both other simulations and experimental data. While this is beyond the scope of the current work (and would nonetheless, cloud our methodological presentation), we note that the specific system we discussed in this paper has been compared against other models from the same class of simulations (varying various physical properties) and also against both simulations and experiments in both two and three dimensional dense granular systems. In all cases, the mechanism responsible for the observed dynamics has proved to be the same, and the same as what we studied here.

ACKNOWLEDGMENTS

This work was funded by a Hong Kong University Grants Council grant under the General Research Fund: grant number PolyU 5262/11E. This work was partially supported by US Army Research Office (W911NF-11-1-0175), the Australian Research Council (DP0986876 and DP120104759) and the Melbourne Energy Institute (AT, DMW). MS is supported by an Australian Research Council Future Fellowship (FT110100896) and would like to thank the Melbourne Energy Institute for travel support. We thank Dr John Peters for useful discussions and Mr Tuan Tran for the software implementation to calculate local Lyapunov exponents.

[1]K. H. Roscoe, A. N. Schofield, and C. P. Wroth, "On the yielding of soils," Géotechnique **8**, 22–53 (1958).
[2]L. Rothenburg, and N. P. Kruyt, "Critical state and evolution of coordination number in simulated granular materials," Int. J. Solids Struct. **41**, 5763–5774 (2004).
[3]A. A. Peña, A. Lizcano, F. Alonso-Marroquin, and H. J. Herrmann, "Biaxial test simulations using a packing of polygonal particles," Int. J. Numer. Analyt. Meth. Geomech. **32**, 143–160 (2008).
[4]S. DJ. Mesarovic, J. M. Padbidri, and B. Muhunthan, "Micromechanics of dilatancy and critical state in granular matter," Géotechnique Lett. **2**, 61–66 (2012).
[5]Z.-Y. Yin and C. S. Chang, "Non-uniqueness of critical state line in compression and extension conditions," Int. J. Numer. Analyt. Meth. Geomech. **33**, 1315–1338 (2009).
[6]X. Zhao, and T. M. Evans, "Numerical analysis of critical state behaviors of granular soils under different loading conditions," Granular Matter **13**, 751–764 (2011).
[7]M. A. Mooney, R. J. Finno, and M. G. Viggiani, "A unique critical state for sand,?" J. Geophys. Geoenviron. Eng. **124**, 1100–1108 (1998).
[8]J. Desrues and G. Viggiani, "Strain localization in sand: An overview of the experimental results obtained in Grenoble using stereophotogrammetry," Int. J. Numer. Analyt. Meth. Geomech. **28**, 279–321 (2004).
[9]F. Alonso-Marroquin and I. Vardoulakis, "Micromechanics of shear bands in granular media," Powders Grains **1**, 701–704 (2005).
[10]F. Alonso-Marroquin, I. Vardoulakis, H. J. Herrmann, D. Weatherley, and P. Mora, "Effect of rolling on dissipation in fault gouges," Phys. Rev. E **74**, 031306 (2006).
[11]C. Marone, "Laboratory-derived friction laws and their application to seismic faulting," Annu. Rev. Earth Planet. Sci. **26**, 643–696 (1998).
[12]J. Krim, P. Yu, and R. P. Behringer, "Stick-slip and the transition to steady sliding in a 2D granular medium and a fixed particle lattice," Pure Appl. Geophys. **168**, 2259–2275 (2011).

[13]T. G. Sitharam and J. S. Vinod, "Critical state behaviour of granular materials from isotropic and rebounded paths: DEM simulations," Granular Matter **11**, 33–42 (2009).
[14]T.-T. Ng, "Discrete element method simulations of the critical state of a granular material," Int. J. Geomech. **9**, 209–216 (2009).
[15]A. Tordesillas, J. Shi, and J. F. Peters, "Isostaticity in Cosserat continuum," Granular Matter **14**, 295–301 (2012).
[16]S. Luding and E. Perdahcioglu, "A local constitutive model with anisotropy for various homogeneous 2D biaxial deformation modes," Chem.- Ing.- Tech. **83**, 672–688 (2011).
[17]V. Magnanimo and S. Luding, "A local constitutive model with anisotropy for ratcheting under 2D axial-symmetric isobaric deformation," Granular Matter **13**, 225–232 (2011).
[18]D. Bi, J. Zhang, B. Chakraborty, and R. P. Behringer, "Jamming by shear," Nature **480**, 355–358 (2011).
[19]A. Tordesillas, D. M. Walker, G. Froyland, J. Zhang, and R. P. Behringer, "Transition dynamics and magic-number-like behavior of frictional granular clusters," Phys. Rev. E **86**, 011306 (2012).
[20]A. Tordesillas, J. Zhang, and R. P. Behringer, "Buckling force chains in dense granular assemblies: physical and numerical experiments," Geomech. Geoeng. **4**, 3–16 (2009).
[21]F. Takens, "Detecting strange attractors in turbulence," Lect. Notes Math. **898**, 366–381 (1981).
[22]M. Small, *Applied Nonlinear Time Series Analysis: Applications in Physics, Physiology and Finance*, Nonlinear Science Series A (World Scientific, Singapore, 2005), Vol. 52.
[23]J. Maquet, C. Letellier, and L. A. Aguirre, "Global models from the Canadian lynx cycles as a direct evidence for chaos in real ecosystems," J. Math. Biol. **55**, 21–39 (2007).
[24]M. Small and C. Carmeli, "Re-examination of evidence for low-dimensional chaos in the Canadian lynx data," in: International Symposium on Nonlinear Theory and its Applications, Research Society of Nonlinear Theory and its Applications, IEICE, 2009.
[25]A. Tordesillas, "Force chain buckling, unjamming transitions and shear banding in dense granular assemblies," Philos. Mag. **87**, 4987–5016 (2007).
[26]A. Tordesillas, D. M. Walker, and Q. Lin, "Force cycles and force chains," Phys. Rev. E **81**, 011302 (2010).
[27]A. Tordesillas, Q. Lin, J. Zhang, R. P. Behringer, and J. Shi, "Structural stability and jamming of self-organized cluster conformations in dense granular materials," J. Mech. Phys. Solids **59**, 265–296 (2011).
[28]M. Muthuswamy and A. Tordesillas, "How do interparticle contact friction, packing density and degree of polydispersity affect force propagation in particulate assemblies?," J. Stat. Mech.: Theory Exp., P09003 (2006).
[29]A. Tordesillas and M. Muthuswamy, "On the modelling of confined buckling of force chains," J. Mech. Phys. Solids **57**, 706–727 (2009).
[30]M. Oda and K. Iwashita, "Study on couple stress and shear band development in granular media based on numerical simulation analyses," Int. J. Eng. Sci. **38**, 1713–1740 (2000).
[31]Y. Guo and J. K. Morgan, "Influence of normal stress and grain shape on granular friction: Results of discrete element simulations," J. Geophys. Res. B, [Solid Earth Planets] **109**, 1–16, doi:10.1029/2004JB003044 (2004).
[32]P. A. Cundall and O. D. L. Strack, "A discrete numerical model for granular assemblies," Géotechnique **29**, 47–65 (1979).
[33]H. D. I. Abarbanel, *Analysis of Observed Chaotic Data* (Springer-Verlag, New York, 1996).
[34]H. D. I. Abarbanel and M. B. Kennel, "Local false nearest neighbours and dynamical dimensions from observed chaotic data," Phys. Rev. E **47**, 3057–3068 (1993).
[35]R. Brown, P. Bryant, and H. D. I. Abarbanel, "Computing the Lyapunov spectrum of a dynamical system from an observed time series," Phys. Rev. A **43**, 2787–2806 (1991).
[36]K. Judd and A. Mees, "Embedding as a modelling problem," Physica D **120**, 273–286 (1998).
[37]M. Small and C. Tse, "Optimal embedding parameters: A modelling paradigm," Physica D **194**, 283–296 (2004).
[38]K. Judd and A. Mees, "On selecting models for nonlinear time series," Physica D **82**, 426–444 (1995).
[39]M. Small and K. Judd, "Comparison of new nonlinear modelling techniques with applications to infant respiration," Physica D **117**, 283–298 (1998).
[40]M. Small and C. Tse, "Minimum description length neural networks for time series prediction," Phys. Rev. E **66**, 066701 (2002).
[41]J. Rissanen, *Stochastic Complexity in Statistical Inquiry* (World Scientific, Singapore, 1989).
[42]K. Judd and M. Small, "Towards long-term prediction," Physica D **136**, 31–44 (2000).
[43]M. Small, K. Judd, and A. Mees, "Modeling continuous processes from data," Phys. Rev. E **65**, 046704 (2002).
[44]M. Small and K. Judd, "Correlation dimension: A pivotal statistic for non-constrained realizations of composite hypotheses in surrogate data analysis," Physica D **120**, 386–400 (1998).
[45]J. Theiler, S. Eubank, A. Longtin, B. Galdrikian, and J. D. Farmer, "Testing for nonlinearity in time series: The method of surrogate data," Physica D **58**, 77–94 (1992).
[46]C. Diks, "Estimating invariants of noisy attractors," Phys. Rev. E **53**, R4263–R4266 (1996).
[47]D. Yu, M. Small, R. G. Harrison, and C. Diks, "Efficient implementation of the Gaussian kernel algorithm in estimating invariants and noise level from noisy time series data," Phys. Rev. E **61**, 3750–3756 (2000).
[48]X.-K. Xu, J. Zhang, and M. Small, "Superfamily phenomena and motifs of networks induced from time series," Proc. Natl. Acad. Sci. U.S.A. **105**, 19601–19605 (2008).
[49]R. V. Donner, M. Small, J. F. Donges, N. Marwan, Y. Zou, and J. Kurths, "Recurrence-based time series analysis by means of complex network methods," Int. J. Bifurcation Chaos Appl. Sci. Eng. **21**, 1019–1046 (2011).
[50]M. Newman, *Networks: An Introduction* (Oxford University Press, 2010).
[51]R. Xiang, J. Zhang, X.-K. Xu, and M. Small, "Multiscale characterization of recurrence-based phase space networks constructed from time series," Chaos **22**, 013107 (2012).
[52]M. Small, D. Yu, and R. G. Harrison, "Observation of a period doubling bifurcation during onset of human ventricular fibrillation," Int. J. Bifurcation Chaos Appl. Sci. Eng. **13**, 743–754 (2003).
[53]M. Oda, T. Takemura, and M. Takahashi, "Microstructure in shear band observed by microfocus x-ray computed tomography," Geotechnique **54**(8), 539–542 (2004).
[54]A. L. Rechenmacher, "Grain-scale processes governing shear band initiation and evolution in sands," J. Mech. Phys. Solids **54**, 22–45 (2006).
[55]A. Tordesillas, G. Hunt, and J. Shi, "A characteristic length scale in confined elastic buckling of a force chain," Granular Matter **13**, 215–218 (2011).